Surface tension, large scale thermodynamic data generation and vapor-liquid equilibria of real compounds

Stefan Eckelsbach[1], Svetlana Miroshnichenko[1], Gabor Rutkai[1], and Jadran Vrabec[1]

1 Introduction

The surface tension of oxygen and nitrogen was calculated using molecular dynamics simulation. Due to the inhomogeneity of the system, the long range correction approach of Janeček [1] was used. The results regarding the temperature dependence of the surface tension were compared to simulation data by Neyt et al. [2] and experimental data.

Because of simpler statistical analogs of certain thermodynamic properties in different ensembles, often a particular ensemble is used to sample thermodynamic data. Due to the possibility to measure any thermodynamic property, which can be measured in a given statistical mechanical ensemble, in every other statistical ensemble, this is not a very efficient approach. A simulation framework based on this fact was applied to calculate a comprehensive data set. The results were compared to highly accurate equations of state that were parameterized to basically all available experimental data.

In the third part of this work, vapor-liquid equilibria (VLE) of binary mixtures were simulated, regarding four molecules of the cyanide group. Therefore, two new molecular force field models for cyanogen and cyanogen chloride were developed. The models of hydrogen cyanide and acetonitrile were taken from preceding work. The simulated phase equilibria were compared to experimental VLE data. Furthermore, excess properties were predicted for two liquid mixtures, i.e. dimethyl ether + water and ethylene oxide + water.

[1] Lehrstuhl für Thermodynamik und Energietechnik (ThEt), Universität Paderborn, Warburger Str. 100, 33098 Paderborn · Author to whom correspondence should be addressed: J. Vrabec, E-mail: jadran.vrabec@upb.de.

2 Surface tension of oxygen and nitrogen

Two fluids, i.e. O_2 and N_2, were studied with respect to their surface tension. The surface tension is of importance for basically every process containing interface interactions, e.g. adhesion or adsorption. Thus it is also needed as an input property for flow simulations based on the continuum approach, e.g. Direct Numerical Simulation or Large Eddy Simulation.

Because of the direct simulation of the interface, a relatively large number of molecules is needed for such simulations, demanding substantial computing power, i.e. parallel computing and a good scalability of the code. To achieve this, the molecular dynamics simulations were carried out with our simulation code *ls*1 [3], which was designed to make efficient use of highly parallel execution.

For the present simulations, the systems were set up with a liquid phase surrounded by a vapor phase. The system thus forms two interfaces, where a direct calculation of the surface tension can be done. After an initial equilibration period, the density profile over the length of the simulation volume remained constant as shown exemplary in Fig. 1 for O_2 at a temperature of 120 K.

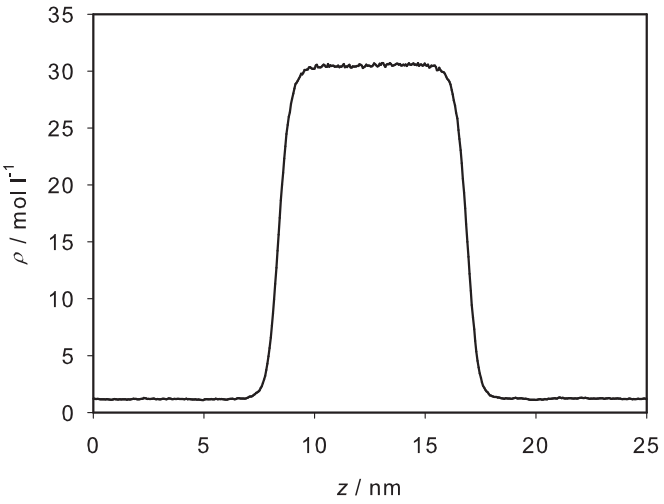

Fig. 1 Density profile of O_2 over the length of the simulation volume across the phase boundaries. The temperature was set to 120 K. After the equilibration of the system, which took 2 ns, the production run was carried out for another 2 ns.

Due to the inhomogeneity of the simulated systems, the long range correction of Janeček [1] was used. The surface tension can be calculated by using the virial approach according to Irving and Kirkwood [4]

$$\gamma = \frac{1}{2A}\left(2\Pi_{zz} - (\Pi_{xx} + \Pi_{yy})\right), \tag{1}$$

where A is the area of the interface and Π is the virial tensor, which is defined as

$$\Pi_{\alpha\beta} = \left\langle \frac{1}{2} \sum_{i=1}^{N} \sum_{j=1}^{N} r_{ij}^{\alpha} f_{ij}^{\beta} \right\rangle . \tag{2}$$

The upper indices α and β represent the x-, y- or z-directions of the distance vector $\boldsymbol{r}_{ij}$ and the force vector $\boldsymbol{f}_{ij}$, in each case between molecules i and j.

The results of the simulations are shown in Fig. 2. They are compared to the simulations of Neyt et al. [2] and experimental data from an equation of state [5]. The present data show a good agreement with the results of Neyt et al., however both molecular simulations slightly overestimate the surface tension in comparison to the experimental data.

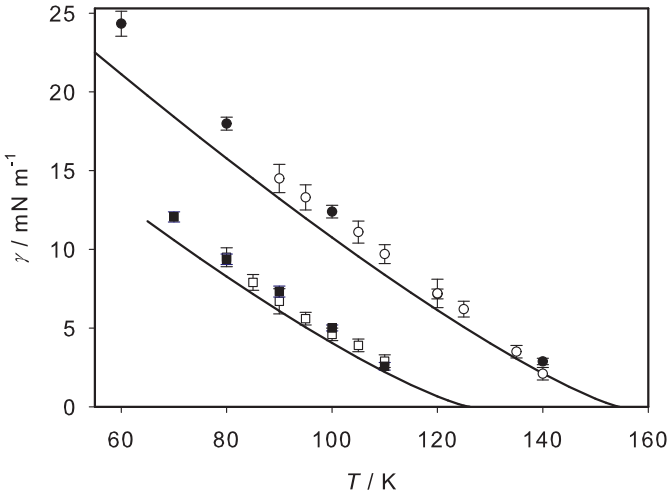

Fig. 2 Surface tension as a function of the temperature for nitrogen and oxygen. oxygen: this work (●), simulations of Neyt et al. [2] (○), equation of state [5] (——); nitrogen: this work (■), simulations of Neyt et al. [2] (□), equation of state [5] (——). The statistical uncertainties of the simulation data are given as the standard error on a 95 % confidence interval.

3 Strategies for large scale thermodynamic data generation

Almost every effort that aims at technological process design and optimization requires a sufficient amount of reliable thermodynamic data. Despite the extensive effort that was invested in measurements over more than a century, the data availability today is still surprisingly low. Among the about 1000 chemical pure compounds

that are in technological use, a complete thermodynamic knowledge is available for about 10 [6], and advanced but still limited knowledge is available for less than 100 [7]. Considering mixtures, where the number of relevant systems is orders of magnitude larger, the data availability is much worse.

Recent progress in molecular simulation has shown that molecular force fields have powerful predictive capabilities with respect to thermodynamic data [8]. Such information can also be straightforwardly accessed for fluids and states which are experimentally too costly or difficult to investigate. Moreover, molecular simulation allows for the generation of comprehensive data sets containing consistent information on arbitrary thermodynamic properties at low cost. At first look, however, the generation of extensive data sets that contain as many different thermodynamic properties as possible may be cumbersome. This is mostly likely caused by the misconception standard textbook approaches in the molecular simulation literature tend to indicate, i.e. certain special techniques or specific statistical mechanical ensembles are required to obtain particular thermodynamic properties. It is true that certain properties have simpler statistical analogs in certain ensembles, nonetheless, any thermodynamic property that can be measured in a given statistical mechanical ensemble can also be measured in any other statistical mechanical ensemble. This is a direct consequence of the physical equivalence of various forms of the thermodynamic fundamental equation, e.g. entropy $S(N,V,E)$, internal energy $E(N,V,S)$, enthalpy $H(N,p,S)$, Helmholtz energy $F(N,V,T)$ or Gibbs energy $G(N,p,T)$, etc., where N is the number of particles, V is the volume, p is the pressure and T is the temperature.

Independent on which form is chosen, any other thermodynamic property can be obtained as a combination of derivatives of the chosen expression with respect to its independent variables. The thermodynamic potential $F/T(N,V,T)$ is a convenient option because it has the advantage that its independent variables can be easily controlled both in the laboratory environment and in molecular simulation. It is therefore a standard choice in empirical fundamental equations of state (FEOS) development [7]. The molecular simulation framework proposed by Lustig [9] offers any A_{mn} to be calculated concurrently from a single NVT ensemble simulation at a given state point for $m,n > 0$, where

$$\frac{\partial^{m+n} F/RT}{\partial^m (1/T) \partial^n (N/V)} \equiv A_{mn}. \tag{3}$$

The internal energy, the pressure, the heat capacities, the speed of sound and any other static thermodynamic property can be built up as a combination of these derivatives [7].

Because experimental measurements cannot satisfy the dire need for raw thermodynamic data in process design due to cost and time inefficiency, molecular simulation can be the answer for this problem. With respect to parameter settings, the NVT ensemble is particularly convenient, because the simulation does not require human interaction or significant attention to parameters during calculation. Thus, in order to produce an extensive data set consisting of as many state points as possible,

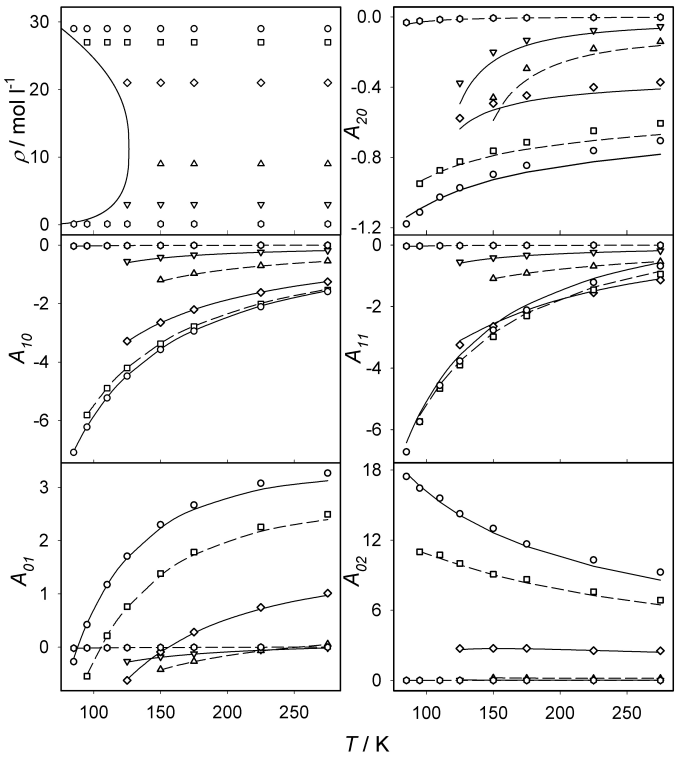

Fig. 3 Distribution of the simulated state points on the temperature vs. density plane (top left) and calculated A_{mn} values as a function of temperature from Monte Carlo molecular simulation (remaining subfigures) for nitrogen. State points were selected excluding the two phase region. Each symbol represents an individually simulated state point using the molecular model of Vrabec et al. [10]. The different symbols denote various isochores. The lines correspond to the FEOS by Span et al. [11]. The statistical uncertainty of the simulation data does not exceed the symbol size.

the only limiting factor is the computation time. Each state point can be sampled with individual and independent calculations making this problem an ideal scenario for high performance computing. Two examples can be seen in Figs. 3 and 4 for nitrogen and acetone, respectively. It can be concluded that there is a good overall agreement between the FEOS and the prediction by molecular simulation. The full data set contains nine different A_{mn} at each state point, from which five are shown in Figs. 3 and 4, covering the entire homogeneous fluid region of technological interest. Due to the current state of high performance computing, such data set can already be obtained within a single day.

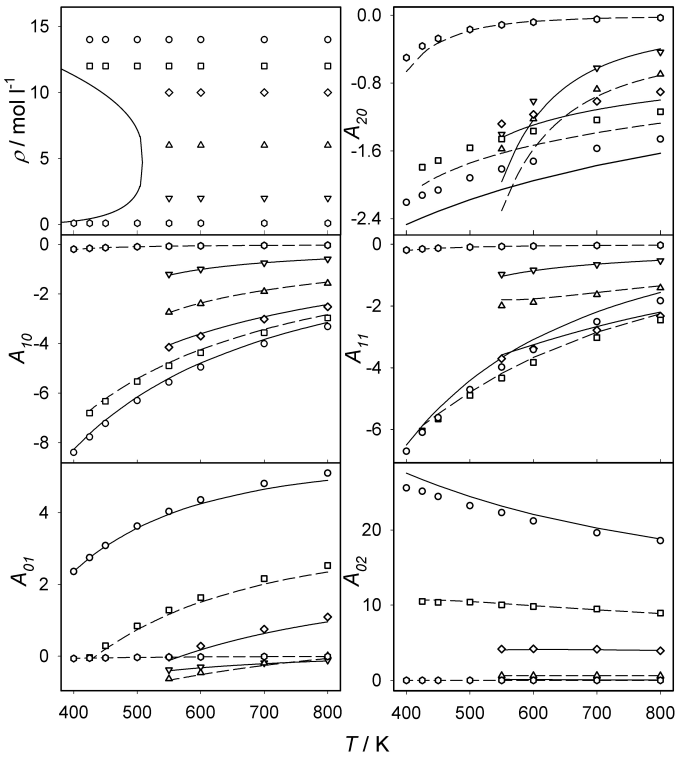

Fig. 4 Distribution of the simulated state points on the temperature vs. density plane (top left) and calculated A_{mn} values as a function of temperature from Monte Carlo molecular simulation (remaining subfigures) for acetone. State points were selected excluding the two phase region. Each symbol represents an individually simulated state point using the molecular model of Windmann and Vrabec [12]. The different symbols denote various isochores. The lines correspond to the FEOS Lemmon and Span [13]. The statistical uncertainty of the simulation data does not exceed the symbol size.

4 Cyanides

Cyanides are chemical compounds that contain the cyano group N≡C-R. Cyanides, including hydrogen cyanide, cyanogen, cyanogen chloride and acetonitrile, are used industrially in the production of synthetic rubbers and plastics as well as in electroplating, case-hardening of iron and steel and fumigation. Many cyanides are highly toxic and have been used throughout history as a poison. Due to the safety issues associated with the handling of cyanides, molecular modeling and simulation can play a particularly important role for the investigation of the thermodynamic properties of these fluids.

The present molecular models include three groups of potential parameters. These are the geometric parameters, specifying the positions of different interaction sites, the electrostatic parameters, defining the polar interactions in terms of point charges, dipoles or quadrupoles, and the dispersive and repulsive parameters, determining the attraction by London forces and the repulsion by electronic orbital overlaps. Here, the Lennard-Jones (LJ) 12-6 potential [14, 15] was used to describe the dispersive and repulsive interactions. The total intermolecular interaction energy thus writes as

$$U = \sum_{i=1}^{N-1} \sum_{j=i+1}^{N} \left\{ \sum_{a=1}^{S_i^{\mathrm{LJ}}} \sum_{b=1}^{S_j^{\mathrm{LJ}}} 4\varepsilon_{ijab} \left[\left(\frac{\sigma_{ijab}}{r_{ijab}} \right)^{12} - \left(\frac{\sigma_{ijab}}{r_{ijab}} \right)^{6} \right] + \right.$$

$$\sum_{c=1}^{S_i^{\mathrm{e}}} \sum_{d=1}^{S_j^{\mathrm{e}}} \frac{1}{4\pi\varepsilon_0} \left[\frac{q_{ic}q_{jd}}{r_{ijcd}} + \frac{q_{ic}\mu_{jd} + \mu_{ic}q_{jd}}{r_{ijcd}^2} \cdot f_1(\boldsymbol{\omega}_i, \boldsymbol{\omega}_j) + \frac{q_{ic}Q_{jd} + Q_{ic}q_{jd}}{r_{ijcd}^3} \cdot f_2(\boldsymbol{\omega}_i, \boldsymbol{\omega}_j) + \right.$$

$$\left. \left. \frac{\mu_{ic}\mu_{jd}}{r_{ijcd}^3} \cdot f_3(\boldsymbol{\omega}_i, \boldsymbol{\omega}_j) + \frac{\mu_{ic}Q_{jd} + Q_{ic}\mu_{jd}}{r_{ijcd}^4} \cdot f_4(\boldsymbol{\omega}_i, \boldsymbol{\omega}_j) + \frac{Q_{ic}Q_{jd}}{r_{ijcd}^5} \cdot f_5(\boldsymbol{\omega}_i, \boldsymbol{\omega}_j) \right] \right\}, \quad (4)$$

where r_{ijab}, ε_{ijab}, σ_{ijab} are the distance, the LJ energy parameter and the LJ size parameter, respectively, for the pair-wise interaction between LJ site a on molecule i and LJ site b on molecule j. The permittivity of the vacuum is ε_0, whereas q_{ic}, μ_{ic} and Q_{ic} denote the point charge magnitude, the dipole moment and the quadrupole moment of the electrostatic interaction site c on molecule i and so forth. The expressions $f_x(\boldsymbol{\omega}_i, \boldsymbol{\omega}_j)$ stand for the dependence of the electrostatic interactions on the orientations $\boldsymbol{\omega}_i$ and $\boldsymbol{\omega}_j$ of the molecules i and j [16, 17]. Finally, the summation limits N, S_x^{LJ} and S_x^{e} denote the number of molecules, the number of LJ sites and the number of electrostatic sites, respectively.

It should be noted that a point dipole may, e.g. when a simulation program does not support this interaction site type, be approximated by two point charges $\pm q$ separated by a distance l. Limited to small l, this distance may be chosen freely as long as $\mu = ql$ holds. Analogously, a linear point quadrupole can be approximated by three collinear point charges q, $-2q$ and q separated by l each, where $Q = 2ql^2$ [18].

For a given molecule, i.e. for a pure fluid throughout, the interactions between LJ sites of different type were defined here by applying the standard Lorentz-Berthelot combining rules [19, 20].

All molecules studied in the present work do not exhibit significant conformational changes. Hence their internal degrees of freedom were neglected and the molecular models were chosen to be rigid. In a first step, the geometric data of the molecules, i.e. bond lengths, angles and dihedrals, were determined by QC calculations. Therefore, a geometry optimization was performed via an energy minimization using the GAMESS(US) package [21]. The Hartree-Fock level of theory was applied with a relatively small (6-31G) basis set. Intermolecular electrostatic interactions mainly occur due to the static polarity of single molecules that can well be

obtained by QC. Here, the Møller-Plesset 2 level of theory was used that considers electron correlation in combination with the polarizable 6-31G basis set.

Fig. 5 shows the considered molecular models.

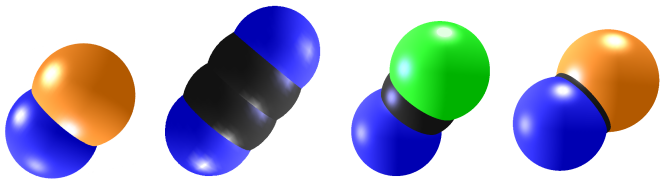

Fig. 5 Snapshot of hydrogen cyanide, cyanogen, cyanogen chloride and acetonitrile (left to right).

Two new molecular force field models are presented for cyanogen and cyanogen chloride, molecular models for hydrogen cyanide and acetonitrile were taken from preceding work [22, 23]. The results for saturated densities obtained with the present models are compared to the available experimental data [25, 26, 27, 28, 29] in Fig. 6.

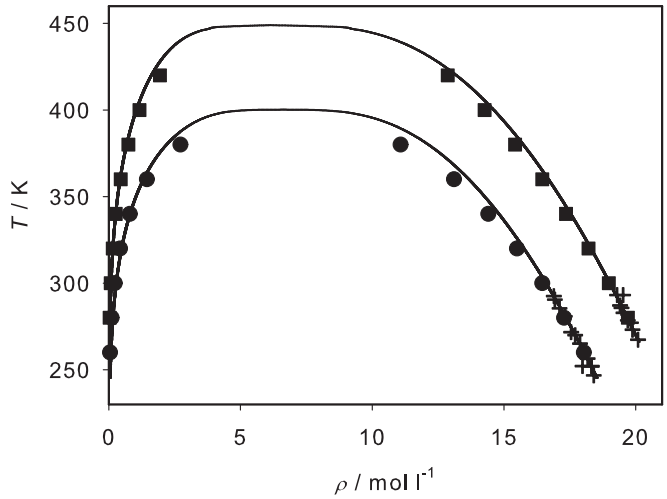

Fig. 6 Saturated densities of cyanogen (●) and cyanogen chloride (■): experimental saturated liquid density [25, 26, 27, 28, 29] (+); DIPPR correlation of experimental data [30] (——). The statistical uncertainties of the present simulation data are within symbol size.

Based on the discussed molecular models, VLE data were predicted for the two binary systems cyanogen chloride + hydrogen cyanide and hydrogen cyanide + acetonitrile. This choice was driven by the availability of experimental VLE data for comparison. The vapor-liquid phase behavior of these binary mixtures was pre-

dicted by molecular simulation and compared to experimental data as well as the Peng-Robinson EOS [24].

Fig. 7 shows the isothermal VLE of cyanogen chloride + hydrogen cyanide at 288.15 K from experiment [31], simulation and Peng-Robinson EOS. The experimental vapor pressure at a liquid mole fraction of x_{NCCl} = 0.5 mol/mol was taken to adjust the binary parameter of the molecular model (ξ = 1.023) and of the Peng-Robinson EOS (k_{ij} = 0.03). It can be seen that the results obtained by molecular simulation agree well with the experimental results and the Peng-Robinson EOS.

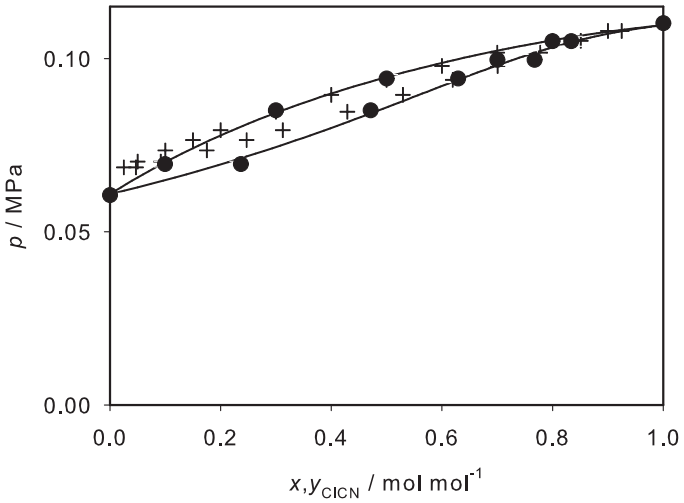

Fig. 7 Isothermal vapor-liquid phase diagram of cyanogen chloride + hydrogen cyanide at 288.15 K: present simulation data with ξ = 1.023 (●); experimental data by Gordon and Benson [31] (+); Peng-Robinson EOS with k_{ij} = 0.03 (——). The statistical uncertainties of the present simulation data are within symbol size.

Fig. 8 shows the isobaric VLE of hydrogen cyanide + acetonitrile at 0.1013 MPa from the experiments by Jiang et al. [32], present simulations and the Peng-Robinson EOS. The binary parameters ξ = 1.02 and k_{ij} = -0.0365 were adjusted to the vapor pressure measured by Jiang et al. [32] at 319.25 K and a liquid mole fraction of x_{HCN} = 0.5174 mol/mol. It can be seen in Fig. 8 that the predictions obtained by molecular simulation with the binary interaction parameter ξ = 1.02 and those from the Peng-Robinson EOS with k_{ij} = -0.0365 agree well with the experimental data.

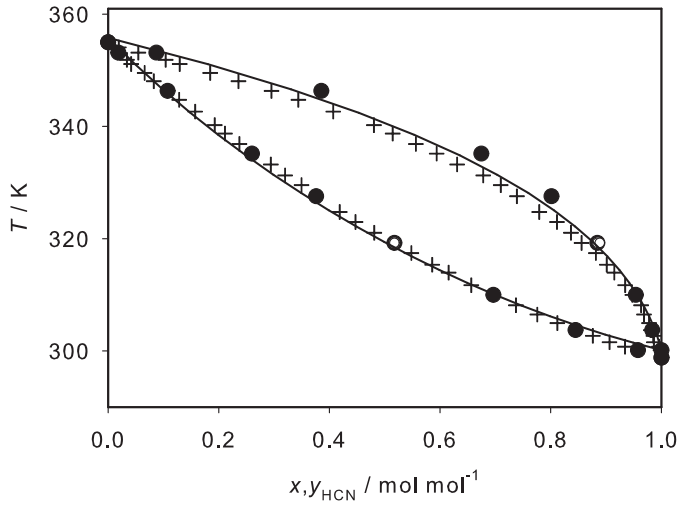

Fig. 8 Isobaric vapor-liquid phase diagram of hydrogen cyanide + acetonitrile at 0.10133 MPa: present simulation data with ξ = 1.02 (●); experimental data by Jiang et al. [32] (+); Peng-Robinson EOS with k_{ij} = -0.054 (——). The statistical uncertainties of the present simulation data are within symbol size.

5 Excess properties

Excess quantities are properties of mixtures which characterize their non-ideal behavior. It is a common practice to characterize liquid mixtures by means of excess mixing functions

$$y^E = y^{mix} - \sum_i x_i y_i, \tag{5}$$

where y^{mix} is the total measured property of the mixture, y_i the molar property of the pure components at the same temperature and pressure and x_i is the mole fraction of component i.

Molecular simulation was used here to predict excess properties of the liquid binary mixtures dimethyl ether + water and ethylene oxide + water. To determine excess properties, a straightforward approach was used. Three simulations at specified temperature and pressure were carried out, two for the pure substances and one for the mixture at a given composition.

Simulation results for the excess enthalpy are shown in Figs. 9 and 10 where they are compared with experimental results [33, 34]. It can be seen that the results obtained by molecular simulation agree well with the experimental results. The excess enthalpy of both mixtures has a peculiar behavior: at the same temperature and pressure, depending on the concentration, the excess enthalpy takes either a positive (endothermic mixing) or a negative (exothermic mixing) value. For both mixtures exothermal mixing effects are notably strong in the water-rich regions.

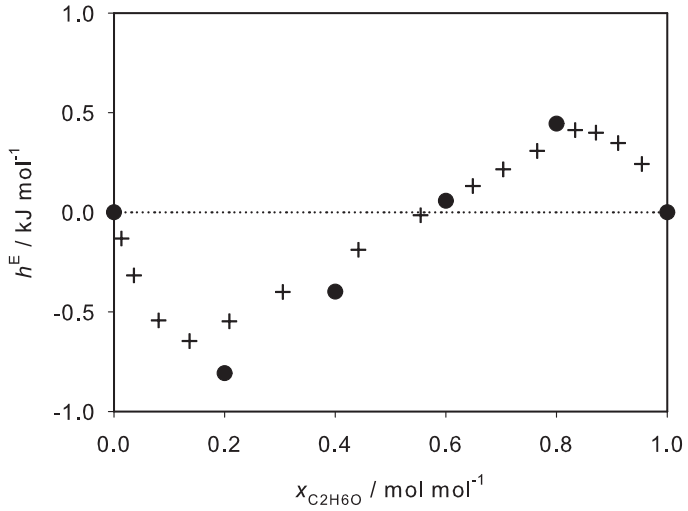

Fig. 9 Excess enthalpy of dimethyl ether + water at 323.15 K and 1.893 MPa: simulation results with ξ = 1.278 (●); experimental data by Park et al. [33] (+). The statistical uncertainties of the present simulation data are within symbol size.

6 Conclusion

The surface tension of oxygen and nitrogen was predicted by molecular dynamics simulation. The results show a good agreement with other molecular simulation work and experimental data.

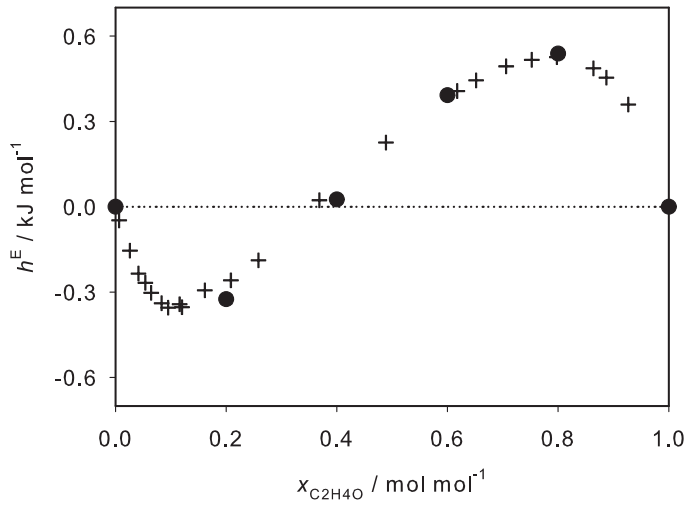

Fig. 10 Excess enthalpy of ethylene oxide + water at 293.15 K and 0.304 MPa: simulation results with ξ = 1.179 (●); experimental data by Glew et al. [34] (+). The statistical uncertainties of the present simulation data are within symbol size.

A simulation framework using a single NVT ensemble simulation to obtain as many thermodynamic values as possible was applied. With this approach, a large data set was created, yielding good agreement with FEOS data for acetone and nitrogen.

Molecular modeling and simulation was used to predict the VLE behaviour of the binary mixtures of cyanogen chloride + hydrogen cyanide and hydrogen cyanide + acetonitrile. For this task, two new molecular models were developed in this work. The used models were able to well reproduce the experimental data.

Also excess properties were studied by molecular simulation, namely the excess enthalpy of dimethyl ether + water and of ethylene oxide + water. Again, a good agreement with experimental data was found.

7 Acknowledgements

We gratefully acknowledge support by Deutsche Forschungsgemeinschaft. This work was carried out under the auspices of the Boltzmann-Zuse Society (BZS) of Computational Molecular Engineering. The simulations were performed on the Cray XE6 (Hermit) at the High Performance Computing Center Stuttgart (HLRS).

References

1. Janeček, J. *J. Phys. Chem. B* **2006**, *110*, 6264-6269.
2. Neyt, J.-C.; Wender, A.; Lachet, V.; Malfreyt, P. *J. Phys. Chem. B* **2011**, *115*, 9421-9430.
3. Buchholz, M.; Bungartz, H.-J.; Vrabec, J. *Journal of Computational Science* **2011**, *2*, 124-129.
4. Irving, J. H.; Kirkwood, J. G. *J. Chem. Phys.* **1950**, *18*, 817-829.
5. Lemmon, E. W.; Penoncello, S. G. *Adv. Cryo. Eng.* **1994**, *39*, 1927-1934.
6. Gubbins, K. E.; Quirke, N. *Molecular Simulation and Industrial Application*; Gordon and Breach: Amsterdam, 1996.
7. Span, R. *Multiparameter Equations of State: An Accurate Source of Thermodynamic Property Data*; Springer Verlag: Berlin, 2000.
8. Industrial fluid properties simulation collective *http://fluidproperties.org*
9. Lustig, R. *Mol. Phys.* **2012**, *110*, 3041-3052.
10. Vrabec, J.; Stoll, J.; Hasse, H. *J. Phys. Chem. B* **2001**, *105*, 12126-12133.
11. Span, R.; Lemmon, E. W.; Jacobsen, R. T; Wagner, W.; Yokozeki, A. *J. Phys. Chem. Ref. Data* **2000**, *29*, 1361-1433.
12. Windmann, T.; Vrabec, J. *in preparation* **2013**.
13. Lemmon, E. W.; Span, R. *J. Chem. Eng. Data,* **2006**, *51*, 785-850.
14. Jones, J. E. *Proc. Roy. Soc.* **1924**, *106A*, 441-462.
15. Jones, J. E. *Proc. Roy. Soc.* **1924**, *106A*, 463-477.
16. Allen, M. P.; Tildesley, D. J. *Computer simulations of liquids*; Oxford University Press: Oxford, 1987.
17. Gray, C. G.; Gubbins, K. E. *Theory of molecular fluids. 1. Fundamentals*; Clarendon Press: Oxford, 1984.

18. Engin, C.; Vrabec, J.; Hasse, H. *Mol. Phys.* **2011**, *109*, 1975-1982.
19. Lorentz, H. A. *Ann. Phys.* **1881**, *12*, 127-136.
20. Berthelot, D. *Compt. Rend. Ac. Sc.* **1898**, *126*, 1703-1706.
21. Schmidt, M. W.; Baldridge, K. K.; Boatz, J. A.; Elbert, S. T.; Gordon, M. S.; Jensen, J. H.; Koseki, S.; Matsunaga, N.; Nguyen, K. A.; Shujun, S.; Windus, T. L.; Dupuis, M.; Montgomery, A. M. *J. Comput. Chem.* **1993**, *14*, 1347-1363.
22. Eckl, B.; Vrabec, J.; Hasse H. *J. Phys. Chem. B* **2008**, *112*, 12710-12721.
23. Deublein, S.; Metzler, P.; Vrabec, J.; Hasse, H. *Mol. Sim.* **2012**, *39*, 109-118.
24. Peng, D. Y; Robinson, D. B. *Ind. Eng. Chem. Fundam.* **1976**, *15*, 59-64.
25. Cook, R. P.; Robinson, P. L. *J. Chem. Soc.* **1935**, *19*, 1001-1005.
26. Ullmann, F.; Gerhartz, W.; Yamamoto, Y. S. *Ullmann's Encyclopedia of Industrial Chemistry*, (5th ed.); VCH Publishers: Weinheim, 1985.
27. Weast, R. C. *Handbook of Chemistry and Physics*, (62nd ed.); The Chemical Rubber Co.: Cleveland, 1981.
28. Steere, N. V. *Handbook of Laboratory Safety*, (2nd ed.); CRC Press: Boca Raton, 1971.
29. Sax, N. I. *Dangerous Properties of Industrial Materials*, (6th ed.); Van Nostrand Reinhold Co.: New York, 1984.
30. Rowley, R. L.; Wilding, W. V.; Oscarson, J. L.; Yang, Y.; Zundel, N. A.; Daubert, T. E.; Danner, R. P. *DIPPR Information and Data Evaluation Manager for the Design Institute for Physical Properties*; AIChE: New York, Version 5.0.2, 2011.
31. Gordon, A. R.; Benson, G. C. *Can. J. Res. B* **1946**, *24*, 285-291.
32. Jiang, W.; Zhang, Y.; Cao, M.; Han, S. *Zhejiang-Daxue-Xuebao* **1983**, *3*, 25-41.
33. Park, S.-J.; Han, K.-J.; Gmehling, J. *J. Chem. Eng. Data* **2007**, *52*, 1814-1818.
34. Glew, D. N.; Watts, H. *Can. J. Chem.* **1971**, *49*, 1830-1840.